LA-UR-19-29173
Approved for public release; distribution is unlimited.

Title: Microstructural and Micromechanical Characterization of FeCrAl C26M tubes

Author(s): Gigax, Jonathan Gregory
Torrez, Avery Jude
Li, Nan

Intended for: Report

Issued: 2019-09-12

Microstructural and Micromechanical Characterization of FeCrAl C26M tubes

Fuel Cycle Research & Development

Prepared for
U.S. Department of Energy
Advanced Fuels Campaign

Jonathan G. Gigax
Avery Torrez
Nan Li

08/08/19

SUMMARY

The present report summarizes the nanoindentation characterization of a FeCrAl alloy, C26M in both tube and bar form. The current heat, AC2-B, investigated by electron backscatter diffraction showed a textured system with the cross-section favoring orientations near the [110] and the tube surface near the [111], similar to previous heats of C26M. Nanoindentation with a Berkovich tip measured a similar moduli and hardness for all specimens of ~220 GPa and ~5 GPa, respectively. Spherical nanoindentation was performed on all specimens and orientations. Indentation with a 100 μm tip resulted in a measured moduli and yield strength values of ~215 GPa and ~1.5 GPa for all specimens, respectively, and in agreement with the Berkovich indentation results. Mesoscale tensile bars were laser cut out of a thin piece of AC2-B. Initial tensile testing showed that a minimum gauge thickness/width of 0.05 mm is required to approach more bulk-like conditions.

TABLE OF CONTENTS

FIGURES

TABLES

Intentionally Blank

1. Introduction

FeCrAl alloys are a class of potential "accident tolerant" fuel cladding candidates to be implemented in light water reactors. Their superior high temperature oxidation resistance, aqueous corrosion resistance, low radiation-induced swelling, and tolerance to loss-of-coolant accident conditions are key factors in their potential integration [1-4] . One major drawback is their comparative large neutron absorption cross-section that requires optimization of fuel cladding thickness and increase in fuel enrichment. However, they possess superior mechanical and thermal properties compared to alternatives (i.e. SiC-based cladding). The ongoing work led by Oak Ridge National Lab has targeted an optimized FeCrAl alloy for tube processing and implementation in light water reactors [5]. Recent characterization of one heat of a FeCrAl alloy, C26M, showed the alloy to have some cold-work that invariably influenced the nanoindentation hardness data [6]. In this study, we perform additional microstructural characterization and nanoindentation analysis on a new C26M heat and provide comparisons with heats received thus far.

2. Materials and Methods

One sample of a C26M tube (Heat #17025001, AC2-B) was obtained and characterized and has a composition given in Table 1. For comparison, we provide EBSD and nanoindentation data of a previous heat, AC1-A. All specimens were ground using successive SiC grit papers down to a grit of 1200. Samples were then polished first using a 0.25 μm diamond solution and finished with a 0.04 μm silica solution.

Table 1. Chemical composition of FeCrAl C26M alloy.

Alloy ID	Fe	Cr	Al	Y	Mo	Si	Nb	C	S	O	N
C26M	bal	11.87	6.22	0.030	1.98	0.2	-	<0.01	0.005	-	-

Scanning electron microscopy of the polished tubes was performed in a FEI Inspect equipped with an EDAX system for acquiring electron backscatter diffraction patterns (EBSD), and obtained with an electron energy of 20 keV. Nanoindentation tests were performed on a Keysight G200 Nanoindenter with a diamond, pyramidal (Berkovich) tip to a final displacement of 2,000 nm with a constant strain rate (loading rate divided by the load) of 0.05 s^{-1}. Continuous stiffness measurements (CSM) were performed at a frequency of 45 Hz and 2 nm displacement amplitude. Hardness and modulus measurements were determined using the Oliver-Pharr method [7]. The tip area function was calibrated by indenting fused silica and using tip properties with a Young's modulus and Poisson's ratio of 1130 GPa and 0.07 (diamond). Spherical nananoindentation tests were performed using two tips with 10 μm and 100 μm radii, respectively. Nanoindentation was performed to a depth of 500 nm using similar system parameters to the nanoindentation with a Berkovich tip. Analysis was performed using a technique outlined by Pathak and Kalidindi [8].

Mesoscale tensile bar specimens we fabricated using the FemtoScribe laser cutting system at the Center for Integrated Nanotechnologies at Los Alamos National Lab. The Femtoscribe is equipped with a Coherent Monaco laser and was operated with a pulse width of 350 fs, wavelength of 1055 nm, repetition rate of 30 kHz, and average energy of 30 μJ.

3. Results and Discussion

3.1 Microstructure

Figure 1 shows IPF maps of the two heats, AC2-B and AC1-A, at different orientations. Here, we focus on the tube/bar cross-section and tube/bar surface for analysis. An illustrative schematic is provided in Fig. 1 for reference. Both heats show similar texture and amounts of cold-work, unsurprising

due to the similar processes used for either. The grain size for both heats of C26M were found to span a range from 10's μm to 100's μm. We note here that compared to a previous generation FeCrAl alloy, B126Y, and the C26M plug, the in grain misorientation is significantly larger. Although we cannot derive a quantitative measure of cold-work from the images, the EBSD maps suggest a matrix that is significantly harder than non-tube or previous generation FeCrAl alloys.

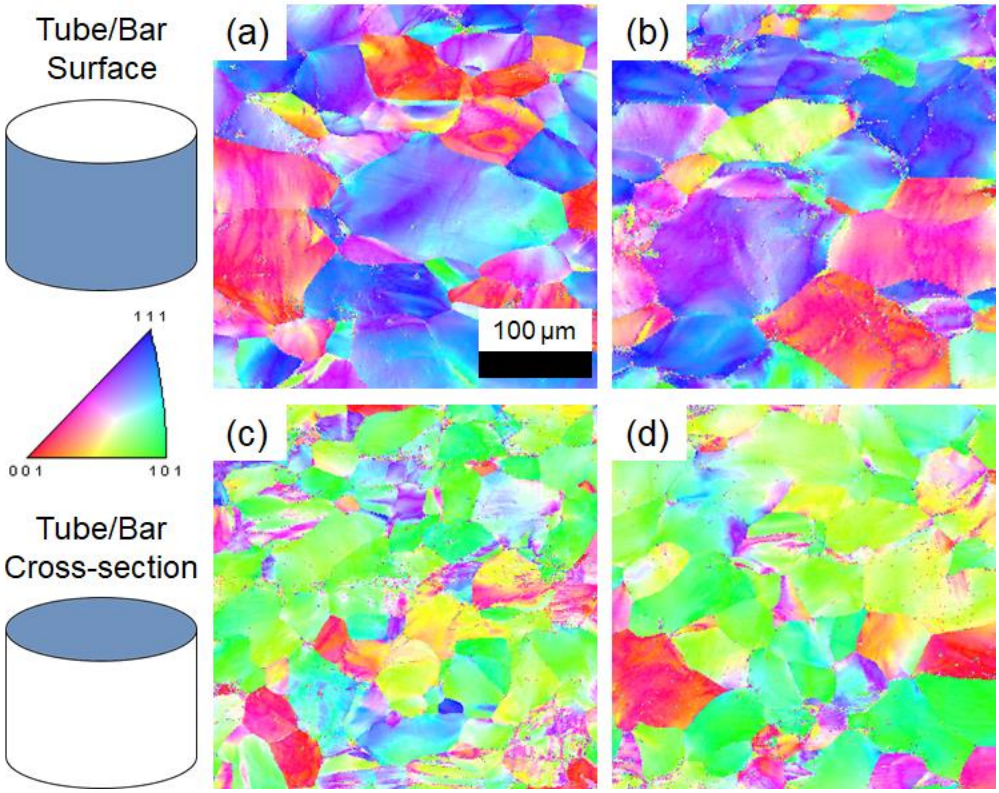

Figure 1 - Inverse pole figure maps for C26M tube surface for heats (a) AC2-B and (b) AC1-A, and C26M tube cross-section for (c) AC2-B and (d) AC1-A. Illustrations of the specimens provided inset on the left-hand side of the figure. Scale bar in (a) applies to all IPF maps.

3.2 Berkovich Nanoindentation

Figure 2 shows representative nanoindentation modulus and hardness curves as a function of depth for the AC2-B tube surface and cross-section. All samples show a similar modulus value of ~220 GPa. Fig. 3b shows that the hardness of the specimens begins to saturate around 500-600 nm below the surface. To avoid the effects of pile-up at deeper depths, the hardness and modulus of the specimens is averaged between a depth of 400-500 nm and, along with the nanoindentation of previous heats, is summarized in Table 2. The AC2-B heat has a modulus similar to other heats and alloy (220 GPa) and a hardness of ~5 GPa.

It is worth noting that the C26M bar shows no major difference between the two orientations examined. We can attribute to the large dislocation content in the grains. Previous heats that possessed a lower misorientation did not show a significant difference in hardness between the surface and cross-section orientations, suggesting that the differences in texture may not play a big role in the hardness. In the case of the AC1-A and AC2-B heats, both effects may be operating in tandem.

Table 2 showcases a range of nanoindentation data obtained through the course of examining several heats and alloys of FeCrAl materials. All alloys here show good agreement with the measured modulus

with slightly higher moduli attributable to cold work in the material. The wide range hardness measured in specimens, however, is significant. Aside from the plug material supplied as part of an assembled cladding tube, no stock material for the C26M prior to tube forming was provided. To establish a baseline hardness/response for tubing, we annealed a C26M tube in a vacuum furnace for 3 hours at 800 °C. The specimen was allowed to cool to room temperature in vacuum. From comparisons against the sets in Table 2, it is clear that the specimen has a hardness significantly lower than other tube specimens. In fact, its hardness is the same as the plug cross-section, indicating that the cold-work in the material is at a similar level to the stock material prior to tube forming.

This result is particularly promising as it provides not only a baseline for annealed tube hardness but also for irradiation hardening behavior. That is, for future irradiations on FeCrAl C26M heats, the change in hardness can be compared against the annealed tube to determine the influence of processing parameters or cold-work on hardness.

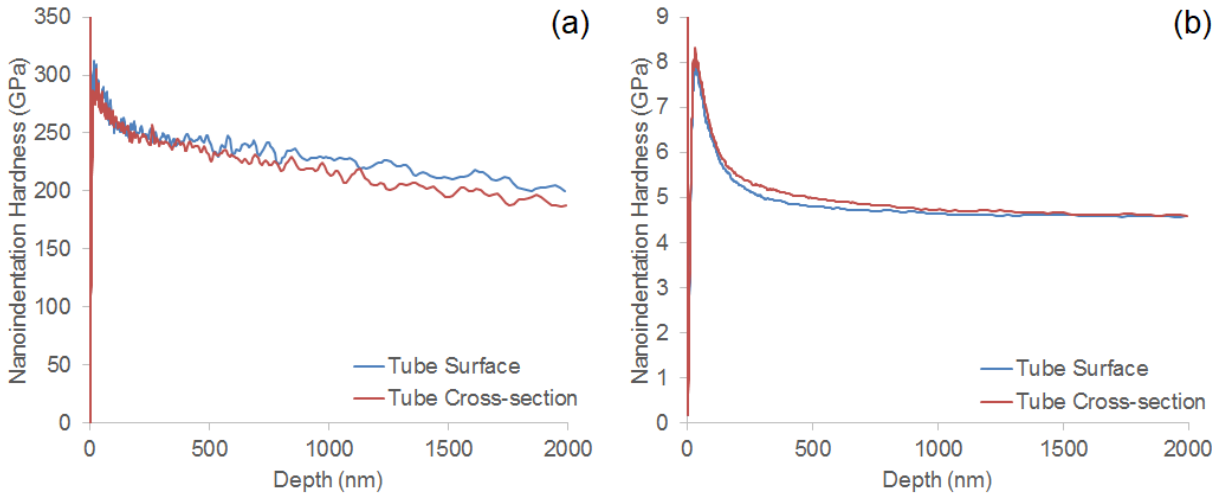

Figure 2 - Nanoindentation (a) modulus and (b) hardness plots as a function of depth for the surface and cross-section of the AC2-B heat.

Table 2. Summary of nanoindentation measurements for FeCrAl alloys and heats investigated thus far. Hardness and modulus averages were made over a displacement range of 400-500 nm. Sample averages come from 20-25 tests spaced 75 µm to place indents in multiple grains.

Specimen	Modulus (GPa)	Modulus Deviation (GPa)	Hardness (GPa)	Hardness Deviation (GPa)
Plug, cross-section	215.9	6.6	3.82	0.11
Plug, surface	214.9	7.8	3.93	0.11
C26M, cross-section	236.5	7.1	4.48	0.12
C26M, surface	249.2	7	4.43	0.14
C26M, 800 °C, 3h anneal	223.6	3.84	3.84	0.1
AC1-A, cross-section	222.7	10.69	4.8	0.26
AC1-A, surface	229.0	8.43	5.2	0.28
AC2-B, cross-section	237.6	6.1	4.87	0.16
AC2-B, surface	232.6	7.2	4.97	0.23

3.3 Spherical Nanoindentation

Fig. 3 provides a comparison of typical nanoindentation stress-strain values for the AC2-B and AC1-A heats. Similar to the Berkovich data, the nanoindentation yield and moduli show little difference between the tube surface and cross-section. Table 3 provides a summary of the spherical nanoindentation results. All specimens had a similar modulus of ~215 GPa and nanoindentation yield strengths of ~1.5 GPa.

One of the main concerns with spherical nanoindentation is that the calculation of nanoindentation stress-strain curves is made based on *a priori* knowledge of a range of moduli the specimen can have (within 20% of value). Coupled with the requirement of a well-defined and clean tip to obtain good elastic data, the technique has limited usefulness. Similar to Berkovich nanoindentation, spherical nanoindentation is a high throughput technique that provides one additional piece of information: compressive strain hardening behavior. It should be, however, interpreted with caution as the test is not uniaxial in nature.

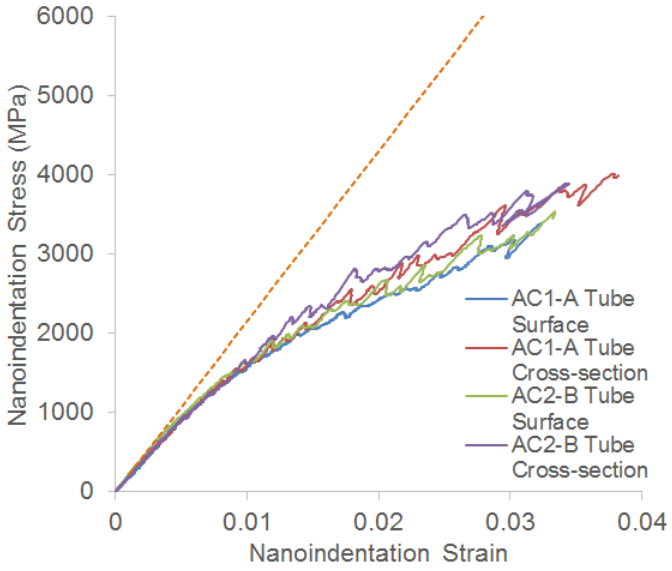

Figure 3 - Typical nanoindentation stress-strain curves of each specimen in this study. A dashed line indicating the modulus is provided for reference.

In order to facilitate the yield strength comparison obtained from spherical nanoindentation to those from macroscale tests, finite element simulations on an isotropic material have shown that the uniaxial and nanoindentation stress states can be related by [9],

$$\sigma = \frac{\sigma_{ind}}{2.2}$$

Where σ_{ind} is the nanoindentation stress state and σ is the uniaxial stress state. This is noted here for comparisons to mesoscale tensile tests that follow in the next section.

3.4 Mesoscale Mechanical Testing

As part of an effort to more fully characterize the mechanical response of the AC2-B heat and future C26M heats, we are in the process of developing tensile testing techniques on the mesoscale. This length scale (i.e. 0.01 to 0.1 mm) has several key advantages. First, the mechanical response typically includes several grain boundaries that provides a more polycrystalline result. Second, the penetration depth of MeV light ions is on this scale. Third, some features or regions are on this scale and enable direct measurement of mechanical properties not accessible by macroscale tensile testing.

For evaluating C26M heats, the goal is to determine the minimum feature size necessary to achieve macroscale results. Our initial attempts so far have focused on a variety of tensile bar sizes including specimens with a gauge width of 0.04 mm and gauge thicknesses of 0.02, 0.03, and 0.05 mm, respectively. These results are shown in Fig. 4. There are striking differences between the yield strength, ultimate tensile strength, and ductility. Furthermore, only the 0.05 mm thick specimen has a significant uniform elongation (~4.5%).

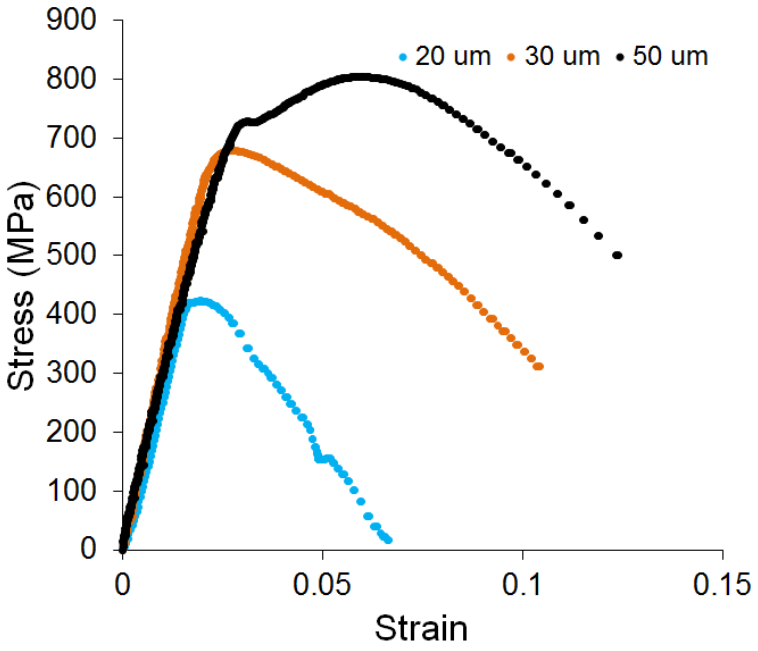

Figure 4 – Engineering stress-strain curves for tensile bars of various sizes of the AC2-B heat.

There are two items worth noting here. First, a previous study showed that the heat-affected zone from laser cutting produces a notable impact on the mechanical properties [10]. The guidance from this study is that the removal of 5 μm of material is needed to achieve a FIB-like response in pure Cu. Due to the lower thermal conductivity of FeCrAl, we speculate that the heat-affected zone is significantly smaller (on the order of 1-2 μm). For the tensile bars in this study, this amounts to ~5% of the volume.

Secondly, the grain size in the specimen is on the order of 60-100 μm. For smaller thicknesses, only a few grains are present in the bar with the failure dictated by a singular grain response. At larger thicknesses, more grain boundaries are present and produce a more polycrystalline response. From Fig. 4, the yield strength of the 50 μm thick specimen shows good agreement with the spherical nanoindentation results (within 10%). We note that both results have yet to be verified by macroscale testing which is currently underway.

4. Conclusions and Future Work

In this study, we have performed characterization of the microstructure of C26M in both tube and bar form. Nanoindentation with a Berkovich tip was utilized to evaluate the hardness of the cross-section and tube surface of both C26M forms. The tube specimens show dramatically higher hardness (4.8-5.2 GPa) than the bar counterparts (~3.9 GPa) with a slight difference between orientations in the tube. This difference was attributed to the fact that the indents on the tube cross-section were placed near the center of the tube wall while the indents on the tube surface were only ~50 μm below the outer surface of the tube.

Spherical nanoindentation was also performed using a large 100 μm spherical tip to avoid pop-in issues. For all specimens, the modulus measured by spherical nanoindentation was ~220 GPa, in agreement with the berkovich measurements. Despite the large number of pop-ins observed in different indents in the C26M bar, the nanoindentation yield strength was measured to be 0.88 and 0.94 GPa for the cross-section and surface, respectively. This was nearly 0.5 GPa lower than the yield strength measured for the C26M tube, similar to the hardness data.

Mesoscale mechanical testing showed a clear impact of size on the yield strength, ultimate tensile strength, uniform elongation, and ductility of tensile bars pulled in the AC2-B heat. The largest specimen with a gauge cross-section of 40 μm x 50 μm showed the best response with the yield closely matching that measured by spherical nanoindentation.

The differences between the tube and bar, and between the tube orientations suggests that some form of tube annealing will be required for more systematic studies. For a comparison of mechanical property changes after ion irradiation to previous FeCrAl alloys or other systems, or even with different tubes of the same heat, a baseline with little cold-work is needed.

5. References

1. R.B. Rebak, K.A. Terrani, W.P. Gassmann, J.B. Williams, K.L. Ledford. Improving Nuclear Power Plant Safety with FeCrAl Alloy Fuel Cladding, MRS Advances (2017) 1-8.
2. Y. Yamamoto, B.A. Pint, K.A. Terrani, K.G. Field, Y. Yang, L.L. Snead. Development and property evaluation of nuclear grade wrought FeCrAl fuel cladding for light water reactors, J Nucl Mater 467, Part 2 (2015) 703-716.
3. K.G. Field, M.N. Gussev, Y. Yamamoto, L.L. Snead. Deformation behavior of laser welds in high temperature oxidation resistant Fe–Cr–Al alloys for fuel cladding applications, J Nucl Mater 454 (2014) 352-358.
4. S.J. Zinkle, K.A. Terrani, L.L. Snead. Motivation for utilizing new high-performance advanced materials in nuclear energy systems, Current Opinion in Solid State and Materials Science 20 (2016) 401-410.
5. Y. Yamamoto, Z. Sun, B.A. Pint, K.A. Terrani. Optimized Gen-II FeCrAl cladding production in large quantity for campaign testing. Oak Ridge: Oak Ridge National Laboratory, 2016.
6. J. Gigax, J. S. Weaver, and N. Li. Microstructural Characterization of FeCrAl C26M Tubes. Los Alamos, NM: Los Alamos National Lab, 2017.
7. W.C. Oliver, G.M. Pharr. Measurement of hardness and elastic modulus by instrumented indentation: Advances in understanding and refinements to methodology, J Mater Res 19 (2004) 3-20.
8. S. Pathak, S. R. Kalidindi. Spherical nanoindentation stress-strain curves. Mater. Sci. Eng. R 91 (2015) 1-36.
9. D.K. Patel, S.R. Kalidindi. Correlation of spherical nanoindentation stress-strain curves to simple compression stress-strain curves for elastic-plastic isotropic materials using finite element models. Acta Mater. 112 (2016) 295-302.
10. J. G. Gigax, H. Vo, Q. McCulloch, M. Chancey, Y. Wang, S. A. Maloy, N. Li, P. Hosemann, Micropillar compression response of femtosecond laser-cut single crystal Cu and proton irradiated Cu, Scripta Mater. 170 (2019) 145-149.